Title
THE CHEMISTRY AND STATUS OF RECHARGEABLE MOLTEN-SALT BATTERIES

Author
Cairns, E.J. .

Publication Date
1933-05-01

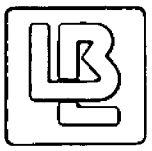

APPLIED SCIENCE DIVISION

Presented at the 163rd Meeting of the Electrochemical Society, San Francisco, CA, May 8-13, 1983; and published in the Proceedings of the Fourth International Symposium on Molten Salts, Vol. 84-2, M. Blander, D.S. Newman, G. Mamantov, M-L. Saboungi, and K. Johnson, Eds., The Electrochemical Society, Inc., 1984

THE CHEMISTRY AND STATUS OF RECHARGEABLE MOLTEN-SALT BATTERIES

E.J. Cairns, G. Mamantov, R.P. Tischer, and D.R. Vissers

May 1983

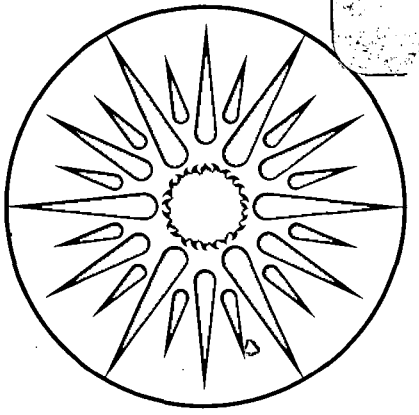

APPLIED SCIENCE DIVISION

Prepared for the U.S. Department of Energy under Contract DE-AC03-76SF00098

DISCLAIMER

THE CHEMISTRY AND STATUS OF RECHARGEABLE MOLTEN-SALT BATTERIES

Elton J. Cairns[a], Gleb Mamantov[b], Ragnar P. Tischer[c],
and Donald R. Vissers[d]

a. Lawrence Berkeley Laboratory, and University of California, Berkeley, CA 94720

b. University of Tennessee, Knoxville, TN 37996

c. Ford Motor Company, Dearborn, MI 48121

d. Argonne National Laboratory, Argonne, IL 60439

Presented at the

Fourth International Symposium on Molten Salts
163rd Meeting of The Electrochemical Society
San Francisco, California

May 8-13, 1983

This work was supported by the U.S. Department of Energy
under Contract DE-AC03-76SF00098

THE CHEMISTRY AND STATUS OF RECHARGEABLE MOLTEN-SALT BATTERIES

Elton J. Cairns[a], Gleb Mamantov[b], Ragnar P. Tischer[c], and Donald R. Vissers[d]

a. University of California, Berkeley, CA 94720
b. University of Tennessee, Knoxville, TN 37996
c. Ford Motor Company, Dearborn, MI 48121
d. Argonne National Laboratory, Argonne, IL 60439

ABSTRACT

The chemistry and the state of development of rechargeable molten salt cells and batteries of current interest are reviewed in this chapter.

INTRODUCTION

Molten-salt cells offer the most attractive combination of high specific energy (100-200 Wh/kg), high specific power (50-200 W/kg), and long cycle life (300-1500 cycles) of any rechargeable cells under investigation at this time. It is these important features that justify the development and application of cells that have the disadvantages of operation at elevated temperatures, and difficult materials problems.

There are two major categories of molten-salt cells: those in which the molten salt is the sole electrolyte, and those in which the molten salt serves as a reactant and as an auxiliary electrolyte (the main electrolyte is a solid). In the first category are such cells as Liℓ/Liℓ-Kℓ/FeS, Liℓ/Liℓ-Kℓ/FeS_2, and Li_4Si/Liℓ-Kℓ/FeS_2; in the second category are Na/$Na_2O{\cdot}xA\ell_2O_3$/Na_2S_n-S, Na/Na^+ glass/Na_2S_n-S, Na/$Na_2O{\cdot}xA\ell_2O_3$/$SC\ell_3A\ell C\ell_4$ in $NaC\ell$-$A\ell C\ell_3$, and Li/Li_2O/$LiNO_3$-KNO_3/V_2O_5. These cells have operating temperatures ranging from 150 to 475°C, and all must be sealed from the atmosphere because of the alkali metal reactants and hydrolytic degradation of molten salt electrolytes.

In this chapter, we will review the relevant chemistry of several of the systems mentioned above, and the state of development of rechargeable cells and batteries based on those systems.

CELLS WITH MOLTEN SALTS AS THE SOLE ELECTROLYTE

The Liℓ/Liℓ-Kℓ/FeS Cell:

This cell makes use of a solid lithium-aluminum alloy as the negative electrode. It supplies lithium as the reactant; the aluminum serves primarily to immobilize the lithium and store it in a solid form at cell operating temperature (450-475°C). The most recent phase diagram of the Li-Aℓ system[1] indicates that at the cell operating temperature (400-460°C) the solubility limit of lithium in aluminum is 10 at.%, which is the boundary of the α-Aℓ phase field. The β-Li-Aℓ field has a composition width of 9 at.% lithium (47-56 at.%). The electrode is normally cycled across the two-phase region between 10 and 47 at.% lithium, within which the emf of the electrode at 450°C is constant at 292 mV relative to lithium.[2,3] As the lithium content is increased above 47 at.% into the β-phase, the potential decreases steeply and approaches that of lithium.[3,4]

The positive electrode of this cell is iron monosulfide. The chemistry of the FeS electrode has been the subject of considerable research, much of it focused at Argonne National Laboratory (ANL). Recently, Tomczuk et al.,[5] published a definitive paper on the phases formed in the electrode, the phase sequence during charge and discharge, and the thermodynamics of the electrochemical and chemical reactions occurring in the electrode, as well as electrolyte effects on such reactions. As much of the earlier work[6-10] was discussed and cited in this paper, it was used as the principal source of information for this review, unless stated otherwise.

Five phases have been identified in the FeS electrode when operated in Li$C\ell$-K$C\ell$ electrolyte: FeS, $LiK_6Fe_{24}S_{26}C\ell$ (≡J-phase), Li_2FeS_2 (≡X-phase), Li_2S and Fe. The FeS phase corresponds to a fully charged cell, the J- and X-phases are present at intermediate states of charge and discharge, and the Fe and Li_2S phases are present in the fully discharged state. Figure 1 shows the ternary Li-Fe-S phase diagram for 450°C, on which all of the phases just mentioned (except J-phase) can be located. Line H-M of Figure 1 represents the pathway of the overall electrode composition as the cell is discharged.

Using the Gibbs phase rule for condensed systems and the fact that all the FeS electrode phases can be prepared from five components: Li$C\ell$, K$C\ell$, Li_2S, Fe and FeS, it was found that for a given Li^+/K^+ ratio in the electrolyte and a given temperature, only two sulfide phases can be in equilibrium; therefore, six such combinations of four sulfide phases result in six possible electrode discharge reactions. These reactions are as follows:

$$26FeS + Li^+ + 6K^+ + C\ell^- + 6e^- \rightarrow J + 2Fe \quad [1]$$
$$J + 25Li^+ + 20e^- \rightarrow 13X + 11Fe + 6K^+ + C\ell^- \quad [2]$$
$$J + 51Li^+ + 46e^- \rightarrow 26Li_2S + 24Fe + 6K^+ + C\ell^- \quad [3]$$
$$2FeS + 2Li^+ + 2e^- \rightarrow X + Fe \quad [4]$$
$$FeS + 2Li^+ + 2e^- \rightarrow Li_2S + Fe \quad [5]$$
$$X + 2Li^+ + 2e^- \rightarrow 2Li_2S + Fe \quad [6]$$

In an actual electrode, different regions are not always in equilibrium with one another. For example, it will occasionally be necessary to consider mixtures of three sulfide phases with iron. Such mixtures can be at equilibrium in a given electrolyte at only one temperature. At other temperatures in the same electrolyte, the three sulfide phases are not in equilibrium, and a chemical reaction tends to consume one of them. The four possible chemical reactions are:

$$23X + Fe + 6KC\ell \rightarrow J + 20Li_2S + 5LiC\ell \quad [7]$$
$$3X + 20FeS + Fe + 6KC\ell \rightarrow J + 5LiC\ell \quad [8]$$
$$23FeS + 3Li_2S + Fe + 6KC\ell \rightarrow J + 5LiC\ell \quad [9]$$
$$FeS + Li_2S \rightarrow X \quad [10]$$

In their work, Tomczuk, et al., used extensive emf and cyclic voltammetric measurements combined with metallographic examinations of the electrode to determine the electrode phase sequence during charge and discharge.

Metallographic examinations of the electrodes showed that during the first discharge, when large particles of FeS are present, the discharge of the particle proceeds in four successive stages: (1) FeS on the surface discharged to J-phase and iron, (2) FeS in the core discharged to X-phase and iron, (3) X-phase in the core discharged to Li_2S and iron, and (4) J-phase on the surface discharged to Li_2S and iron. Because the formation of J-phase was limited by diffusion and the discharge of J-phase was found to be a slow, lower-voltage reaction, suppressing these reactions and accentuating the X-phase reaction seemed desirable.

One method found and implemented to decrease the stability of J-phase was to increase the Li^+/K^+ ratio of the electrolyte, which tends to drive the chemical reactions [7]-[9] to the left.[6,7] Saboungi, et al., investigated the stability of J-phase and the effect that the $\overline{Li^+/K^+}$ ratio has on the stability of J-phase, using both an electrochemical titration method[6] and a metallographic reaction product-examination method.[7]

A first discharge of FeS in LiCℓ-saturated (68 mol % LiCℓ) electrolyte at 425°C indicated the J-phase surface layer generated under these conditions was only one fifth as thick as the surface layers generated under similar conditions in the eutectic (~58 mol % LiCℓ) electrolyte.[5] Vissers, et al.,[9] in tests of small FeS cells found the active material utilization of FeS electrodes improved

markedly as the LiCℓ content of electrolyte was increased above that of the eutectic. From these cell studies, it was apparent that the LiCℓ-rich electrolyte (68 mol % LiCℓ-32 mol % KCℓ) permitted recharge of the electrode at a low voltage (~1.55 V, IR-included) and discharge of the electrode at high current densities (50-100 mA/cm^2). Consequently, this electrolyte composition was taken to be an optimum and it is referred to as LiCℓ-rich electrolyte. This electrolyte is now routinely used in 300 Ah cells.

To determine the phase sequence in the FeS electrode during charge and discharge, cyclic voltammetric, emf, and metallographic studies were conducted on the FeS electrode both in the eutectic and in the LiCℓ-rich electrolytes.[5] These studies were conducted with well-cycled electrodes where the particle size of the active electrode material was <20μm.

The phase sequence determined for the electrode during charge and discharge in the eutectic and LiCℓ-rich electrolytes is summarized in Figure 2. In this figure, the Roman numerals indicate the sequence of electrochemical reactions, while the broad arrows indicate the chemical reactions.

In the eutectic electrolyte, the charge sequence found was I_C, $Li_2S \rightarrow X$; II_C, $X \rightarrow FeS$; chemical reactions [7] $X \rightarrow J + Li_2S$, [8] $FeS + X \rightarrow J$ and III_C, $J \rightarrow FeS$. The $X \rightarrow J + Li_2S$ chemical reaction is believed to be minimal. On discharge, the sequence was I_D, $FeS \rightarrow J$; II_D, $FeS \rightarrow X$, III_D, $J \rightarrow X$;. IV_D, $X \rightarrow Li_2S$; V_D, $J \rightarrow Li_2S$ (Note that each phase discharges by multiple pathways). The chemical reactions [7] and [8] or $X \rightarrow Li_2S$ and J, and $FeS \rightarrow X \rightarrow J$ are superimposed on the electrochemical discharge pathways.

In the LiCℓ-rich electrolyte, the phase sequence during charge is very similar to that in the eutectic electrolyte, except that the chemical reactions forming J-phase are greatly reduced. The result is an electrode that is much more readily charged. On discharge, the electrochemical phase sequence is similar to that found in the eutectic electrolyte, except that J-phase may now react chemically with Li_2S to form X-phase, a material with fast electrochemical kinetic properties.

Phase transition potentials were measured in an investigation on the thermodynamic properties of the FeS electrode system in LiCℓ-KCℓ eutectic electrolyte.[5] For three of the phase transitions: E_3(J - X), E_4 (J - Li_2S) and E_7 (X - Li_2S), the emf of the FeS electrode was measured at appropriate states of charge and discharge. In making such measurements, an emf value was extracted from such data only when certain reversibility criteria were satisfied. For example, the $J \rightarrow X$ (E_3) data were obtained at both 20% discharge and 80% charge, which are equivalent states of charge approached from different directions. The agreement in these measurements is an indication of reversibility. To obtain the other three phase-transition potentials, the

emf of the FeS + Li_2S transition was calculated from the available free energy values for (α + β)-Li-Aℓ, FeS and Li_2S; the FeS + X and FeS + J values were then calculated from the thermodynamic interdependence that exists between the potentials. The potentials E_2, E_3, and E_4, which are dependent on electrolyte composition, were then calculated for the LiCℓ-rich (67 mol % LiCℓ) electrolyte from the reaction stoichiometry and the changes in the activity of LiCℓ and KCℓ with electrolyte composition. The regions of phase stability and emf values for the respective transitions in the two electrolyte systems (eutectic and LiCℓ-rich) are summarized in Figures 3 and 4.

Using the emf equations and the activities of LiCℓ and KCℓ, Tomczuk, et al., calculated the temperature at which the emf curves intersect in LiCℓ-saturated electrolyte. The intersection of E_2*, E_5*, and E_3, which occurs at 621°C in eutectic electrolyte, was calculated to occur at 481°C in electrolyte saturated with LiCℓ [75.2 mol % LiCℓ[11]]. This temperature is in excellent agreement with the metallographically determined temperature of 481° ± 5°C.[7] Similar calculations for the intersection of E_3, E_4*, and E_7 (which occurs at 473°C in eutectic electrolyte)provided a value of 429°C in LiCℓ-saturated electrolyte [68.4 mol % LiCℓ[5]], which is in reasonable agreement with the 419° ± 5°C temperature determined in the metallographic studies.[7] The above temperature calculations rely on the reaction stoichiometries and certain emf differences, while the metallographic studies only require the presence or absence of phases. The good agreement between these independent methods tends to confirm the emf equations and the reaction stoichiometries. Therefore, the free energy changes of the chemical reactions can be calculated with a reasonable degree of confidence.

The free energy changes of the four chemical reactions were calculated from the thermodynamic relationships between the six electrochemical transition potentials and the free energies. The free energy changes of the chemical reactions are:[5]

$$\Delta G_7^\circ = 322.6 + 0.682T$$
$$\Delta G_8^\circ = -236 + 0.380T$$
$$\Delta G_9^\circ = -223 + 0.336T$$
$$\Delta G_{10}^\circ = 4.32 - 0.015T$$

where the temperatures are in °C and free energy changes are in kJ.

In a more recent study, Tomczuk, et al.,[12] determined the phase transition potentials of the FeS electrode from similar studies in LiF-LiCℓ-LiBr, where the only phase transitions are FeS + X and X + Li_2S. The results of these emf measurements were:

*Indicates the emf has been calculated.

E (in mV), FeS - X = 1338.9 + 0.0133T(K)
E (in mV), X - Li_2S = 1432.11 - 0.147T(K)

These values are in good agreement with their earlier values.[5]

Thermodynamically, one would predict that the principal overcharge reactions of the FeS electrode are as follows:

$$FeS + Fe_{1-x}S + x\ Fe^{+2} + 2xe^- \qquad [11]$$
$$2FeS + FeS_2 + Fe^{+2} + 2e^- \qquad [12]$$

The calculated voltages for these reactions vs. (α + β)-Li-Aℓ at 450°C are 1.84 and 2.17 V, respectively; studies of overcharged FeS electrodes by Tomczuk, et al., confirm the proposed overcharge reactions.[13]

A large number of LiAℓ/LiCℓ-KCℓ/FeS cells of various sizes and designs have been built and operated. A typical cell design is shown in Figure 5. The electrodes are pressed plaques of electrode reactant and powdered electrolyte; the electrolyte between the electrodes is usually held in a boron nitride felt (but sometimes is used in a paste form using MgO powder).[14] Cells of the type shown in Figure 5 having capacities up to about 350 Ah have been tested, and they have demonstrated cycle lives of 250-400, with a few cells surpassing 1000 deep cycles. Specific energy values up to about 100 Wh/kg have been achieved.

A few batteries of LiAℓ/FeS cells have been tested in sizes up to about 4 kWh. The lifetimes, as is to be expected, have been shorter than for single cells. These batteries have shown cycle lives up to about 275.[15] The main cause of failure is the extrusion of the pasty positive electrode active material out of the positive electrode. This extruded material bridges across to the negative electrode, shorting the cell.

Table 1 summarizes the status of cell performance, lifetime, and other features. The recent cell development activities are also summarized, including work on 10-cell batteries, as are the remaining problem areas.

The Li-Si/LiCℓ-KCℓ/FeS_2 Cell:

This cell is closely related to the one discussed just above. It makes use of electrodes that have a much lower equivalent weight, and therefore has a significantly higher specific energy.

The negative electrode of this cell is a solid lithium-silicon alloy, which operates very effectively at practical current densities, and can store up to about four lithium atoms per silicon atom. The Li-Si phase diagram has been subject of several investi-

gations,[16-18] with considerable discrepancy regarding exact phase compositions. According to the most recent work,[19-21] the phases include $Li_{4.4}Si$, $Li_{3.25}Si$, $Li_{2.33}Si$, $Li_{1.71}Si$, and Si. The emf values (vs. Li) for the corresponding phase transitions are 44, 150, 277 and 326 mV, respectively, at 450°C.[16-18] During normal cell operation, the Li-Si electrode is usually operated between the $Li_{3.25}Si$ and Si° sections of the phase diagram to avoid the corrosion and self-discharge problems associated with the $Li_{4.4}Si$-$Li_{3.25}Si$ two-phase region.

The positive electrode of this cell is solid FeS_2. This is an attractive material because it is plentiful, has good electronic conductivity, a reasonably low equivalent weight, rapid reaction rates at cell operating temperature (450°C), and has a sulfur activity such that good potentials are achieved (1.6-2.1 V vs. Li).

The most extensive study of the high-temperature phases in the Li-Fe-S system was conducted by Martin[22,23] who employed metallography to establish the number and identity of the phases and X-ray diffraction to support the phase identification. In his work, Martin developed the Li_2S-FeS-FeS_2 section of the Li-Fe-S phase diagram, which provides an excellent guide for electrochemical investigations. Tomczuk, et al.,[24] have subsequently updated this work on the phase relationships of the FeS_2 electrodes and elucidated their role in the chemistry of the electrode. The updated phase diagram is shown in Figure 1. The major ternary phases in the diagram are indicated by the point F, which is the compound $Li_3Fe_2S_4$ (or $Li_{1.5}FeS_2$), and the field C-D-E, which is a solid solution whose composition can be approximated by $Li_{2+x}Fe_{1-x}S_2$. This field is quite narrow and is best approximated in the diagram by a line, although, of course, it must have some finite width. At X = 0 (point E), this phase has the composition Li_2FeS_2 and it is a major phase in FeS electrodes. At X ≈ 0.2 (point D), the composition is approximately $Li_{2.2}Fe_{0.8}S_2$; this composition is in equilibrium with $Li_3Fe_2S_4$. At X ≈ 0.33 (point C), the composition is $Li_{2.33}Fe_{0.67}S_2$, and the material of this composition is in equilibrium with Li_2S and FeS_2.

The dashed lines A-L and H-M are given in Figure 1 to indicate the equilibrium phase progressions in FeS_2 and FeS electrodes, respectively. [These progressions are only valid, of course, in the absence of phases like $LiK_6Fe_{24}S_{26}Cl$ (which would require a quinary diagram)]. Thus, the dashed line H-M gives FeS → Li_2FeS_2 and Fe → Li_2S and Fe as the predicted phase progression in the FeS electrode, but, as noted before, more complex phase progressions are also known. The dashed line A-L gives as the predicted phase progression in FeS_2 electrodes:

$$FeS_2 \rightarrow Li_3Fe_2S_4 \rightarrow Li_{2+x}Fe_{1-x}S_2 + Fe_{1-x}S \rightarrow Li_2FeS_2 \rightarrow Li_2S + Fe$$

The arrows on the above phase progression are a shorthand notation used by Tomczuk, et al.,[24] for the cell reactions.

The phases found in the room-temperature examinations of the FeS_2 electrodes were FeS_2, $KFeS_2$, $Li_3Fe_2S_4$, $Li_{2.33}Fe_{0.67}S_2$, Li_2FeS_2, $Fe_{1-x}S$, $LiK_6Fe_{24}S_{26}Cl$, Li_2S, and Fe. In metallographic examinations, these phases could be readily distinguished from one another by their color, isotropy, and crystal structure. The X-ray diffraction patterns and crystal systems are presented in this work[24] for the respective phases. If the two potassium-containing compounds, which were present at low levels, are excluded from consideration, the phases identified by Tomczuk, et al.,[24] in the FeS_2 electrodes are in agreement with Martin's phase diagram.

Coulometric discharge data[24] obtained on the FeS_2 electrode also support Martin's phase diagram. The breaks in the discharge curve were located at 37.9, 42.6, and 50% of the total capacity. These values compare well with the breaks predicted by the phase diagram, namely 37.5, 41.8, and 50%, and they indicate that the phase sequence during discharge observed in the FeS_2 electrodes agrees with that predicted by the phase diagram if one neglects the potassium-containing compounds.

The phase sequence during charge was found by Tomczuk, et al.,[24] to be slightly different than that observed during discharge for the $Li_3Fe_2S_4$ - FeS_2 phase transition. During discharge, the $Li_3Fe_2S_4$ formed on the FeS_2; during charge, the FeS_2 formed on the $Fe_{1-x}S$. The phases formed during charge are shown in Table 2. Cyclic voltammetry studies[25] have shown that the discharge begins very near 1.76 V vs. (α + β)-Li-Al, but the charge reaction occurs at 1.82 V; these observations are also supported by the cell data.[24] A nonequilibrium soluble electrode species also seemed to be formed in this transition region during charge,[24] which further suggests that the charge and discharge reactions for this transition must be quite different.

The principal overcharge reaction[25] of the FeS_2 electrode occurs at ~2.4 V vs. (α + β)-Li-Al and is:

$$FeS_2 + 2Cl^- \rightarrow FeCl_2 + 2S + 2e^- \qquad [13]$$

where the formation of sulfur and ferrous chloride increases the porosity of the electrode and decreases the coulombic efficiency of the cell.

A number of Li-Si/FeS_2 cells of various designs have been built and operated at Argonne National Laboratory, and General Motors Research Laboratories. The GM cell was disk-shaped and had the construction shown in Figure 6. Cells of this type had a capacity of about 70 Ah, and had voltage vs. capacity curves as shown in Figure 7.

These cells had lifetimes of up to 16,000 h, and cycle lives of up to about 700 cycles. Only a small amount of work has been performed on batteries of Li-Si/FeS_2 cells. This system is in an earlier stage of development than LiAl/FeS, but offers the possibility of twice the specific energy, as shown in Table 3, which summarizes the status of the Li-Si/FeS_2 cell.

CELLS WITH MOLTEN SALTS AS REACTANT AND AUXILIARY ELECTROLYTE

The $Na/Na_2O{\cdot}xAl_2O_3/Na_2S_n$-S Cell:

This cell makes use of a molten sodium negative electrode; a solid tubular electrolyte of beta alumina ($Na_2O{\cdot}xAl_2O_3$, x = 5 to 11) which conducts sodium ions; and a molten sulfur-sodium polysulfide positive electrode with graphite felt as the current collector. The operating temperature is 350°C. The overall cell reaction can be represented by

$$2Na + xS \rightleftharpoons Na_2S_x \qquad (x = 2 \text{ to } 5) \qquad [14]$$

The reaction at the sulfur electrode

$$(x-1)S_x^{=} + 2e^- \rightleftharpoons xS_{x-1}^{=} \qquad (x = 3 \text{ to } 5) \qquad [15]$$

is followed by equilibration with the free sulfur phase

$$S_{x-1}^{=} + S \rightleftharpoons S_x^{=} \qquad [16]$$

as long as free sulfur exists.

This overview will discuss the Na_2S_2-S phase diagram, some of the properties of sodium polysulfides and the electrochemical reactions at the electrode interface including diffusion and subsequent chemical reactions. Only highlights can be given of facts that are well established and of important questions that are still open.

The phase diagram (Figure 8) has been investigated numerous times.[26-30] The main difficulty in such investigation is that in this system equilibria are established slowly and that sodium polysulfides tend to undercool and solidify as glasses.[31] If the glass is subsequently crystallized, the resulting crystals are not necessarily in equilibrium with the melt at the liquidus line. The salient features of the phase diagram are the existence of the three polysulfides Na_2S_2, Na_2S_4 and Na_2S_5, and a miscibility gap with liquid sulfur and Na_2S_5 saturated with sulfur in equilibrium. This miscibility gap plays an important role in electrode kinetics and

consequently in cell performance. Na_2S_3 is stable at room temperature, but decomposes above 100°C into Na_2S_2 and Na_2S_4, which of course does not preclude its existence in the melt.[32,33]

Attempts have been made to interpret the dependence of the open circuit voltage of the cell on melt composition thermodynamically.[34-36]

One difficulty in analyzing the kinetics in this system is our limited knowledge of the exact composition of the melt, i.e., of the nature of the ions present. However, it has been established that uncharged sulfur is present in the polysulfide melt only in the form of polysulfide ions.[36]

The propensity of polysulfide melts to solidify as glasses was used to advantage in Raman spectroscopy.[33] Investigations at the temperature of the melt gave little insight, because of the coexistence of a series of polysulfides,[37] whereas with glasses interpretable results were obtained. The presence of the ions $S_2^{=}$, $S_4^{=}$, and $S_5^{=}$ in melts of the appropriate composition was confirmed, but the existence of $S_3^{=}$ in the melt is still controversial.

Another difficulty in analyzing the kinetics is the problem of defining diffusion in a pure melt. Earlier approaches used in other systems have been applied here successfully.[38,39] Also, it must be kept in mind that in electrochemical measurements in pure melts without solvent, migration of reactant ions is not negligible, and diffusion coefficients obtained are only effective values. However, these values (around 10^{-6} cm^2/s) agree quite well with those determined by tracer studies.[40] Activation energies are in agreement with those found for melt viscosity.[41-43]

The rate of the interfacial reactions at practical current densities is clearly determined by diffusion. Exchange currents are extremely high. Relaxation methods have yielded values of 1 A/cm^2 with steps up to 400 mV and of more than 10 A/cm^2 with steps of a few millivolts. This may be understood as measuring one and in the former case both of two consecutive steps in the two electron reaction.[38,39]

Kinetics have been investigated by potential sweep chronoamperometry,[38,39] by chronopotentiometry,[44] and by the rotating disk method.[45,46]

The kinetics of the cell reactions are illustrated by Figure 9 of a cyclic potential sweep with melt resistance measured concurrently. Neither anodically nor cathodically do we see a limiting current. On both sides the reaction peak (A,F) is followed by an abrupt decrease

in current caused by an insoluble reaction product: solid Na_2S_2 on the cathodic side (B) and liquid sulfur on the anodic side. The conductance decreases correspondingly. The formation of insoluble products necessitates the use of expanded electrodes in all but very thin layers of polysulfide electrolyte. The reduction peak A has been identified as a superposition of two consecutive one electron reaction peaks. On the return sweep the current always passes through zero at the potential of a melt saturated with Na_2S_2.

It has been suggested that the Randles-Sevcik equation cannot be applied because of formation of these blocking surface layers. However careful analysis has shown that the influence of layer formation becomes noticeable only after the peak has been reached, and the consistent results obtained with Randles-Sevcik analysis bear this out.

The formation of solid Na_2S_2 does not pose a problem in cell operation, especially since the layers seem to be crystalline and not very dense; they in fact inhibit overdischarge. The influence of sulfur formation at the anode depends on the nature of the electrode material, i.e., on its preferential wettability. Carbon and many other materials are preferentially wetted by sulfur. When the melt composition reaches Na_2S_5 and becomes saturated with sulfur, there is no longer a mechanism for the removal of the adsorbed insulating sulfur layer. Current flow is blocked, and the cell cannot be recharged beyond this point. Fortunately there are means of modifying the surface so that it becomes preferentially wetted by polysulfide and permits charge into the two phase region of the phase diagram. Certain metal surfaces (e.g., those of chromium steels) will not block anodic current at all. These surfaces (covered by a corrosion layer) are clearly preferentially wetted by polysulfide. Unfortunately they are not stable enough for use in practical cells.

Basic research stimulated by the invention of the sodium/sulfur cell has established many facts that are essential for the development work. But there are still a few important questions to be solved:

1) the distribution of ion species $S_x^=$ (x = 2 to 6) in sodium polysulfide melts;
2) the actual values of the very high exchange currents at the electrode;
3) the role of migration in the transport process.

Even though there are some unanswered questions about the sulfur-sodium polysulfide electrode, there is enough known to allow high-performance, long-lived cells to be built in significant quantities. Cells of various sizes, recently 65-200 Ah, have been operated, and have demonstrated specific energies of 120-160 Wh/kg, peak specific power values of 100-200 W/kg, and cycle lives of 300-1500. A typical cell design is shown in Figure 10.

Difficulty has been encountered in obtaining full recharge of the sulfur electrode because of the formation of an insulating layer of

sulfur at the sites of the electrochemical reaction. Various schemes were devised for maintaining electrolytic and electronic contact between the solid electrolyte, the polysulfide phase, and the graphite current collector. Some useful approaches have included graded-resistance graphite felt current collectors (to distribute the reaction zone more widely), layered current collectors (graphite felt, well wetted by sulfur, in alternating layers with alumina cloth, well wetted by polysulfide), with the planes of the layers perpendicular to the axis of the electrolyte tube, and additives to sulfur, to improve its electronic conductivity.

A number of batteries of Na/Na_2S_n-S cells have been tested. Figure 11 shows typical charge and discharge curves for a parallel-connected module of 25 cells[47] Most of the batteries have been able to store about 10 kWh, and a recent one has stored 100 kWh. One 25 kWh module of the latter battery has operated for over 600 cycles. This represents the largest and longest-lived high-temperature battery known to these authors.

The status of the work on this system is summarized in Table 4. The remaining problems include corrosion of the metals in contact with the sulfur electrode, the high cost of the electrolyte, seals, and failure of cells during freeze-thaw thermal cycling.

The $Na/Na_2O{\cdot}xAl_2O_3/SCl_3AlCl_4$ in $AlCl_3$-NaCl Cell:

This cell offers an unusually high voltage of 4.2 V, and a theoretical specific energy of 563 Wh/kg, corresponding to the reaction:

$$4Na + SCl_3AlCl_4 + 3AlCl_3 \rightarrow S + 4NaAlCl_4 \qquad [17]$$

It is also possible to discharge the sulfur to the minus-two valence state. In this case, the reactions are:

$$4Na + SCl_3AlCl_4 + 3AlCl_3 \rightarrow S + 4NaAlCl_4 \qquad [17]$$

$$2Na + S + AlCl_3 \rightarrow AlSCl + 2NaCl \qquad [18]$$

In addition, the operating temperature is in the range 180-250°C vs. 350°C for Na/Na_2S_n-S.

As discussed below, Reaction 17 proceeds through several intermediates. The evidence for the reactants, products and the intermediates may be summarized as follows:

1. The Raman spectrum of the melt in the positive electrode compartment of a fully charged cell[48] is a summation of the spectral features of $Al_2Cl_7^-$, $AlCl_4^-$ and SCl_3^+ (the presence of Na^+ ions is, of course, not detected by Raman spectroscopy). The fully charged state may be obtained either by a four electron oxidation of elemental sulfur in the melt or by the addition of the compound SCl_3AlCl_4[49] to an acidic ($AlCl_3$/NaCl molar ratio > 1) melt.

2. Raman spectra taken at different stages of the first discharge plateau clearly show the disappearance of SCl_3^+, the increase of $AlCl_4^-$, and the decrease of $Al_2Cl_7^-$ bands.[48] In fact, the melt compositions estimated from the intensities of the Raman bands of $Al_2Cl_7^-$ and $AlCl_4^-$ are in reasonable agreement with melt compositions calculated from the stoichiometry of the electrochemical process. Thus, the discharge corresponds to a decrease in the modified Lewis acidity of the melt in the positive electrode compartment, in agreement with Equations 17 and 18. Although no clearcut assignments of intermediate species could be made based on Raman spectra, UV-visible and electron spin resonance spectroelectrochemical and electrochemical studies[50-54] of more dilute melt solutions provide evidence for monovalent sulfur species, present as S_2Cl_2 or possibly S_2Cl^+, and, in $AlCl_3$-rich melts, for cations such as S_8^{2+}, S_5^+ and S_8^+.[50,51] Thus the overall reduction process of SCl_3^+ involves an increase in S-S bonds and decreasing Cl^- complexation.

3. The end of the first discharge plateau corresponds to the formation of elemental sulfur, present predominantly as S_8.[48,55] The solubility of sulfur in the melt increases with the melt acidity[55] or, in other words, it decreases as the discharge proceeds. Thus, it is likely that in a cell most of the elemental sulfur is present as a suspension.

4. The product formed during the second discharge plateau depends on whether the melt is acidic or basic (this will usually correspond to $NaAlCl_4$ saturated with NaCl[56]). In acidic melts polymeric $(AlSCl)_n$ is formed, while in basic melt polymeric $(AlSCl_2^-)_n$ is present.[48,57] The values of n are believed to be ~3-4 in dilute melts.[57] There is no evidence for the formation of polysulfide ions in $AlCl_3$-NaCl melts, although Raman evidence for the S_3^- ion in basic $AlCl_3$-CsCl melts has been obtained.[58]

The electrochemistry of sulfur oxidation and reduction has been investigated in very acidic ($AlCl_3$/NaCl, 63/37 mole %) melts,[52] melts of intermediate pCl (where pCl is defined as $-\log [Cl^-]$),[54] and in $AlCl_3$/NaCl melts saturated with NaCl.[53] These investigations, as well as spectroelectrochemical studies in 63/37 $AlCl_3$/NaCl melts,[51] were performed in more dilute melts than is normally the case for cell studies.

In very acidic melts the oxidation of sulfur to SCl_3^+ involves three voltammetrically distinguishable steps. The first of these steps results in S_8^+ and probably S_8^{2+} and S_5^+;[51] the apparent n-value per sulfur atom ranges from 0.13 to 0.22 depending on the temperature (175-250°C) and the concentration of sulfur. The second step results in the formation of monovalent sulfur which is oxidized to

SCl_3^+ in the third step. Spectroelectrochemical studies[51] point to the formation of S_4^{2+} and divalent sulfur as intermediates in the second and third oxidation steps. The low oxidation states of sulfur, such as S_8^+ and S_8^{2+}, were found to be unstable in slightly acidic melts (pCl < 3.8);[54] only two voltammetric steps are observed corresponding to the formation of S_2Cl_2 and SCl_3^+. In NaCl-saturated melts SCl_3^+ is unstable; the main oxidation product is S_2Cl_2.[53]

A number of simple glass laboratory cells of up to twenty ampere hours capacity have been operated, and a few metal-cased cells have been tested.[59,60] Some voltage vs. capacity curves for a cell employing both Reactions 17 and 18 above are shown in Figure 12. The upper plateau corresponds to Reaction 17; the lower plateau corresponds to Reaction 18. This cell used a reticulated vitreous carbon current collector in the positive electrode. Tungsten spirals have also been used.

Recent work with this cell has demonstrated that high power densities (up to 788 mW/cm^2 at 360 mA/cm^2 and 2.2 V) can be achieved. Some cells of this type have demonstrated cycle lives in excess of 400 cycles, and one small cell (0.56 Ah) was operated for 1370 cycles (with the positive electrode inside the β''-Al_2O_3 tube).

Values for specific energy and specific power of complete cells cannot be quoted because no cells of practical design have been constructed yet. The status of this cell is summarized in Table 5. The problems include: highly corrosive positive electrode material; significant vapor pressure of $AlCl_3$; seals; poor wetting of the electrolyte by sodium requires special start-up procedures.

CONCLUSIONS

Based upon the material presented in this paper, the following conclusions may be drawn.

1. Molten-salt rechargeable cells are making good progress in their evolution into high-performance, long-lived batteries.
2. The chemistry and electrochemistry of these systems are complex, but are reasonably well understood.
3. Materials problems are significant for these systems, and could well be the pace-setting issues in their development.
4. The field of molten salts offers interesting opportunities for the development of new electrochemical cells. More are sure to follow.

REFERENCES

1. J. L. Settle and K. M. Myles, "The Lithium-Aluminum Phase Diagram," in Argonne National Laboratory Report ANL-76-9 (April 1976), p. 42.
2. N.P. Yao, L. A. Heredy, and R. C. Saunders, J. Electrochem. Soc., 118, 1039 (1971).
3. C. J. Wen, B. A. Boukamp, R. A. Huggins, and W. Weppner, J. Electrochem. Soc., 126, 2258 (1970).
4. J. R. Selman, D. K. DeNuccio, C. J. Sy, and R. K. Steunenberg, J. Electrochem. Soc., 124, 1160 (1977).
5. Z. Tomczuk, S. K. Preto, and M. F. Roche, J. Electrochem. Soc., 128, 761 (1981).
6. M. L. Saboungi, J. J. Marr, and M. Blander, J. Electrochem. Soc., 125, 1567 (1978).
7. M. L. Saboungi and A. E. Martin, Abs. 339, The Electrochemical Society Extended Abstracts, Pittsburgh, PA, October 15-20 (1978), p. 919.
8. R. A. Sharma, J. Electrochem. Soc., 123, 448 (1976).
9. D. R. Vissers, K. E. Anderson, C. K. Ho, and H Shimotake, "Effects of the LiCl-KCl Electrolyte Composition on the Performance of the Positive Electrode in Li-Al/FeS Cells," in Proceedings of the Symposium on Battery Design and Optimization, Vol. 79-1, S. Gross, ed., The Electrochemical Society, Princeton (1979), p. 416.
10. F. C. Mrazek and J. E. Battles, J. Electrochem. Soc., 124, 1556 (1977).
11. B. Chu and J. Egan, Ann. NY Acad. Sci., 79, 908 (1960).
12. Z. Tomczuk, M. F. Roche, and D. R. Vissers, J. Electrochem. Soc., 128, 2255 (1981).
13. Z. Tomczuk, A. E. Martin, and R. K. Steunenberg, Abs. 47, The Electrochemical Society Extended Abstracts, Las Vegas, NV, October 17-22 (1976), p. 131.
14. D. L. Barney, R. K. Steunenberg, A. A. Chilenskas, E. C. Gay, J. E. Battles, R. Hudson, B. A. Askew, and F. C. Tompkins, "Lithium/Iron Sulfide Batteries for Electric-Vehicle Propulsion and Other Applications," Argonne National Laboratory Report ANL-81-65 (February 1982).
15. W. E. Miller, E. C. Gay, and D. Kilsdonk, in Proceedings of the 17th Intersociety Energy Conversion Engineering Conference, Institute of Electrical and Electronic Engineers, New York, 1982, P. 585.
16. F. A. Shunk, Constitution of Binary Alloys, Second Supplement, McGraw-Hill Book Co., New York (1969), p. 480.
17. R. A. Sharma and R. N. Seefurth, J. Electrochem. Soc., 123, 1763 (1976).
18. S. C. Lai, J. Electrochem. Soc., 123, 1196 (1976).
19. H. G. von Schnering, R. Nesper, K. F. Tebbe, and J. Curda, Z. Metall., 71, 357 (1980).

20. C. J. Wen and R. A. Huggins, J. Solid State Chem., 37, 271 (1981).
21. B. A. Boukamp, G. C. Lesh, and R. A. Huggins, J. Electrochem. Soc., 128, 725 (1981).
22. A. E. Martin, in "High Performance Batteries for Electric-Vehicle Propulsion and Stationary Energy Storage," Argonne National Laboratory Report ANL-78-94 (1980), p. 167.
23. A. E. Martin and Z. Tomczuk, in "High-Performance Batteries for Electric Vehicle Propulsion and Stationary Energy Storage," Argonne National Laboratory Report ANL-79-39 (1979), p. 71.
24. Z. Tomczuk, B. Tani, N. C. Otto, M. F. Roche, and D. R. Vissers, J. Electrochem. Soc., 129, 925 (1982).
25. S. K. Preto, Z. Tomczuk, S. von Winbush, and M. F. Roche, J. Electrochem. Soc., 130, 264 (1983).
26. T. G. Pearson and P. L. Robinson, J. Chem. Soc., 132, 1473 (1930).
27. N. K. Gupta and R. P. Tischer, J. Electrochem. Soc., 119, 1033 (1972).
28. D. G. Oei, Inorg. Chem., 12, 435 (1973).
29. E. Rosén and R. Tegman, Chem. Scripta, 2, 221 (1972).
30. E. A. Mayorova, N. M. Romanchenko, and A. G. Morachevskii, Electrokhimiya, 17, 523 (1981).
31. G. J. Janz and D. J. Rogers, The Electrochemical Society Extended Abstracts, 82-2, No. 333.
32. D. G. Oei, Inorg. Chem. 12, 438 (1973).
33. G. J. Janz, J. R. Downey, G. J. Wasilczyk, J. W. Coutts, and A. Elouard, Inorg. Chem., 15, 1759 (1976).
34. A. G. Morachevskii, M. A. Bykova, and L. N. Gerasimenko, Zh. Fiz. Khim., 45, 2066 (1971).
35. H. S. Wroblowa, The Electrochemical Society Extended Abstracts, 82-2, No. 332.
36. B. Cleaver and A. J. Davies, Electrochim. Acta, 18, 733 (1973).
37. B. Cleaver and S. J. Sime, Electrochim. Acta, 28, 703 (1983).
38. R. P. Tischer and F. A. Ludwig, Adv. Electrochem. & Electrochem. Eng., 10, 391 (1977).
39. D. A. Aikens in The Sulfur Electrode, R. P. Tischer, ed., Academic Press, in press.
40. J. Divisek, F. G. Bodewig, J. Mergel, H. Lippert, and B. Kastening, J. Electrochem. Soc., 127, 357 (1980).
41. B. Cleaver, A. J. Davies, and M. Hames, Electrochim. Acta, 18, 719 (1973).
42. B. Cleaver and A. J. Davies, Electrochim. Acta, 18, 727 (1973).
43. B. Cleaver in The Sulfur Electrode, R. P. Tischer, ed., Academic Press, in press.
44. K. D. South, J. L. Sudworth, and J. G. Gibson, J. Electrochem. Soc. 119, 554 (1972).
45. R. D. Armstrong, T. Dickinson, and M. Reid, Electrochim. Acta, 20, 709 (1975).
46. R. D. Armstrong, T. Dickinson, and M. Reid, Electrochim. Acta, 21, 935 (1976).

47. Ford Aerospace & Communications Corporation, Annual DOE Review of the Sodium-Sulfur Battery Program, April 22, 1980.
48. K. Tanemoto, A. Katagiri, and G. Mamantov, J. Electrochem. Soc., 130, 890 (1983).
49. G. Mamantov, R. Marassi, F. W. Poulsen, S. E. Springer, J. P. Wiaux, R. Huglen, and N. R. Smyrl, J. Inorg. Nucl. Chem., 41, 260 (1979).
50. G. Mamantov, V. E. Norvell, and L. Klatt, J. Electrochem. Soc., 127, 1768 (1980).
51. V. E. Norvell, K. Tanemoto, G. Mamantov, and L. Klatt, J. Electrochem. Soc., 128, 1254 (1981).
52. R. Marassi, G. Mamantov, M. Matsunaga, S. E. Springer, and J. P. Wiaux, J. Electrochem. Soc., 126, 231 (1979).
53. R. Marassi, G. Mamantov, and J. Q. Chambers, J. Electrochem. Soc., 123, 1128 (1976).
54. K. Tanemoto, R. Marassi, C. B. Mamantov, Y. Ogata, M. Matsunaga, J. P. Wiaux, and G. Mamantov, J. Electrochem. Soc., 129, 2237 (1982).
55. R. Huglen, F. W. Poulsen, G. Mamantov, R. Marassi, and G. M. Begun, Inorg. Nucl. Chem. Letters, 14, 167 (1978).
56. G. Torsi and G. Mamantov, Inorg. Chem., 10, 1900 (1971).
57. R. W. Berg, S. von Winbush, and N. J. Bjerrum, Inorg. Chem., 19, 2688 (1980).
58. R. Fehrmann, S. Von Winbush, G. N. Papatheodorou, R. W. Berg, and N. J. Bjerrum, Inorg. Chem., 21, 3396 (1982).
59. G. Mamantov, R. Marassi, M. Matsunaga, Y. Ogata, J. P. Wiaux, and E. J. Frazer, J. Electrochem. Soc., 127, 2319 (1980).
60. G. Mamantov, K. Tanemoto, and Y. Ogata, J. Electrochem. Soc., 130, 1528 (1983).

Table 1. Summary of LiAℓ/LiCℓ-KCℓ/FeS Cell

$2LiA\ell + FeS \rightarrow Li_2S + 2A\ell$

E = 1.33 V; 458 Wh/kg Theoretical

T = 450°C

Status

Specific Energy	60-100 Wh/kg @ 30 W/kg
Specific Power	60-100 W/kg, peak
Cycle Life	300+ @ 100% DOD
Lifetime	5000+ h
Cost	>$100/kWh

Recent Work

- Multielectrode cells
- LiX-rich electrolyte
- BN felt separators
- Wetting agent for separators
- Powder separators-MgO
- Freeze-thaw cycling
- Improved current collectors
- Batteries of 320 Ah cells

Problems

- Low specific energy
- Low voltage per cell
- Cell shorting major failure mode
- Electrode swelling and extrusion
- Agglomeration of Li-Aℓ with cycling
- Capacity loss
- High separator cost
- Leak-free feedthroughs
- Thermal control

Table 2. Sulfide Phases During Charge of LiAl/FeS_2 Cells Operated at 410°C Using Eutectic Electrolyte[a]

Cell designation	Charge potential[b] vs. (α + β) LiAl	X-ray findings		Metallographic findings
		Major phase	Minor phase	
Z-1	1.53	Li_2FeS_2	$LiK_6Fe_{24}S_{26}Cl$	Li_2FeS_2 + trace of $LiK_6Fe_{24}S_{26}Cl$
Z-9	1.64	$Li_{2.33}Fe_{0.67}S_2$ and Li_2FeS_2	$Fe_{1-x}S$	Li_2FeS_2 + $Fe_{1-x}S$ + $Li_{2.33}Fe_{0.67}S_2$
Z-2	1.72	$Li_3Fe_2S_4$	None detected	$Li_3Fe_2S_4$ only
Z-7	1.79	$Li_3Fe_2S_4$	None detected	$Li_3Fe_2S_4$ + 5% $Fe_{1-x}S$
Z-3	1.82	$Li_3Fe_2S_4$	FeS_2 + $Fe_{1-x}S$	Not examined
Z-8	1.85	FeS_2	$Fe_{1-x}S$	Fe_2S + $Fe_{1-x}S$

[a] The phases Li_2S and Fe are not shown in this table because they react at a much lower potential of 1.33V to yield Li_2FeS_2.

[b] Cells were constant-current charged at ~18 mA/cm^2 to this potential and then constant voltage charged at this potential for periods in excess of 18hr. Current densities at the end of this time period were <2 mA/cm^2.

Table 3. Summary of $Li_4Si/LiCl$-KCl/FeS_2 Cell

$Li_4Si + FeS_2 \rightarrow 2Li_2S + Fe + Si$

E = 1.8, 1.3 V; 944 Wh/kg Theoretical

T = 450°C

Status

Specific Energy	120 Wh/kg @ 30 W/kg
	180 Wh/kg @ 7.5 W/kg
Specific Power	100 W/kg, peak
Cycle Life	700 @ 100% DOD
Lifetime	~15,000 h
Cost	>$100/kWh

Recent Work

- Bipolar cells
- Li-Si electrodes
- BN felt separators
- 70 Ah cells

Problems

- Materials for FeS_2 current collector
- Leak-free feedthroughs
- High internal resistance
- Low-cost separators needed
- Thermal control

Table 4. Summary of Na/Na^+ Solid/S Cell

$2Na + 3S \rightarrow Na_2S_3$

E = 2.0 V; 758 Wh/kg Theoretical

T = 350°C

Status

Specific Energy	90-180 Wh/kg @ 30 W/kg
Specific Power	60-180 W/kg peak
Cycle Life	300-1500
Lifetime	3000-15,000 h
Cost	>$100/kWh

Recent Work

- Batteries, 10-100 kWh
- C_6N_4 additive to S
- Ceramic (TiO_2) electronic conductors
- Shaped current collectors
- Tailored resistance current collectors
- Sulfur-core cells
- Layered current collectors
- Graphite cladding
- $Na_{1+x}Zr_2Si_xP_{3-x}O_{12}$
- Thermocompression bonded seals

Problems

- Low cost electrolyte
- Corrosion-resistant material for contact with S
- Thermal cycling
- Low cost seals
- Robust electrolyte seals

Table 5

$Na/Na_2O \cdot xAl_2O_3/SCl_3AlCl_4$ in $AlCl_3$-NaCl

$4Na + SCl_3AlCl_4 + 3AlCl_3 \rightarrow 4NaAlCl_4 + S$

E = 4.2 V; 563 Wh/kg Theoretical

T = 250°C

Status: laboratory cells only (4 Ah)

Current Density	20 mA/cm^2 @ 3.5 V
Power Density	790 mW/cm^2 max. @ 2.2 V
Cycle Life	1370 @ 100% DOD
Lifetime	7000 h
Cost	too early

Recent Work

- Larger cells - 20 Ah
- Less expensive current collectors
- Reduction to $S^=$

Problems

- Sodium wetting?
- Vapor pressure of $AlCl_3$
- Corrosion of metals and some electrolytes
- Electrolyte cracking?
- Seals

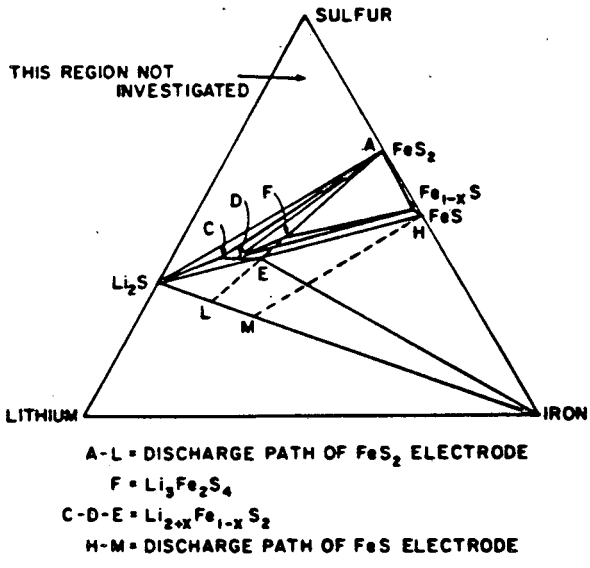

Figure 1. Isothermal section of the Li-Fe-S phase diagram at 450°C.

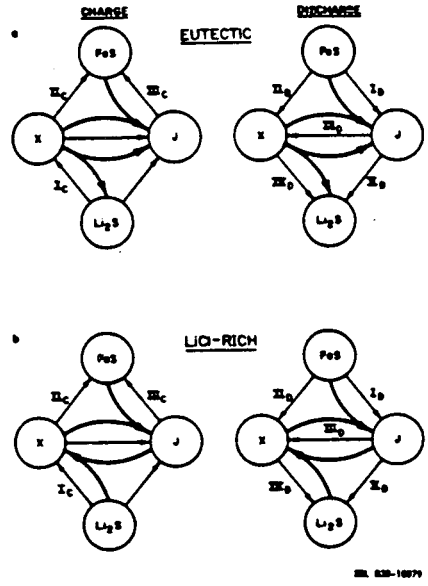

Figure 2. Summary of reaction assignments for two general cases (a) lower LiCl concentrations and temperatures and (b) higher LiCl concentrations and temperatures. Peak assignments from cyclic voltammetry (roman numerals) and the directions of chemical reactions (X ↔ J + Li_2S) and (X + FeS ↔ J) are shown, where X = Li_2FeS_2 and J = $LiK_6Fe_{24}S_{26}Cl$.

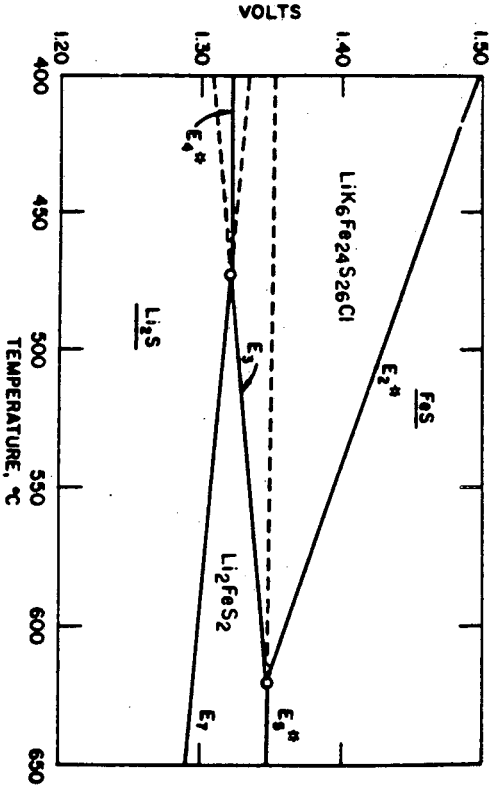

Figure 3. Regions of stability of FeS, $LiK_6Fe_{24}S_{26}Cl$ (djerfischerite or J-phase), Li_2FeS_2 (X-phase), and Li_2S in the LiCl-KCl eutectic. An asterisk indicates a calculated emf.

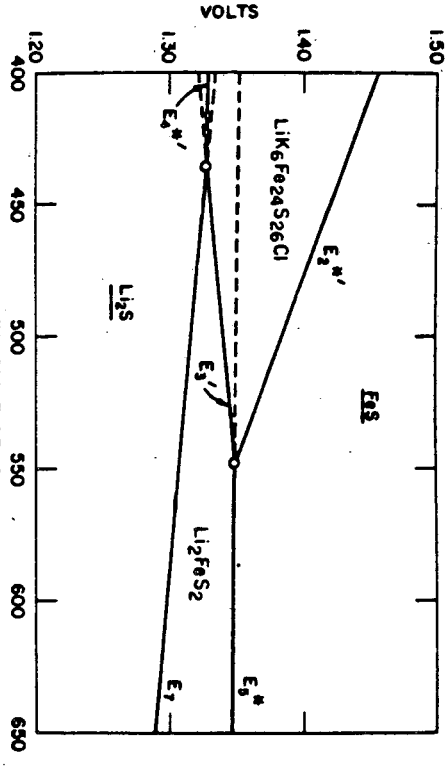

Figure 4. Regions of stability of FeS, $LiK_6Fe_{24}S_{26}Cl$ (J-phase), Li_2FeS_2 (X-phase), and Li_2S in LiCl-rich electrolyte (67 m/o LiCl). An asterisk indicates a calculated emf. Note that E_2*', E_3', and E_4*' are shifted from their corresponding values in eutectic electrolyte.

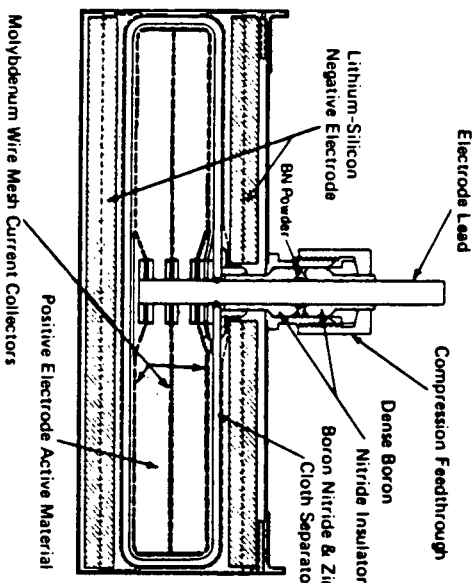

Figure 6. Cross section of a disk-shaped Li_4Si/FeS_2 cell, having about 70-Ah capacity.

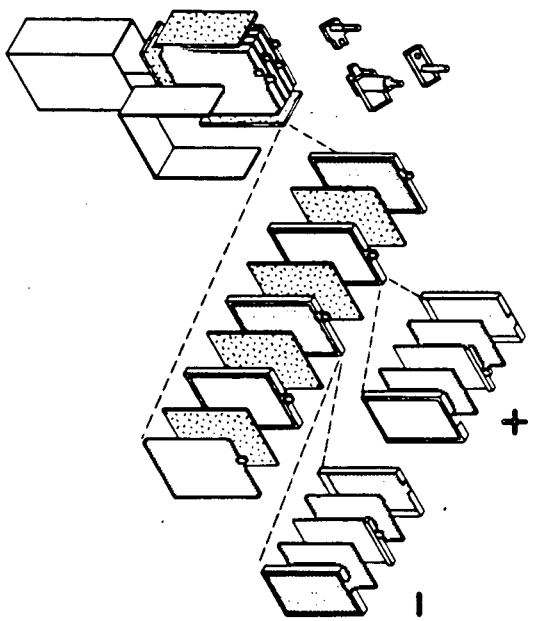

Figure 5. Design used for the immobilized electrolyte/powder separator cells.

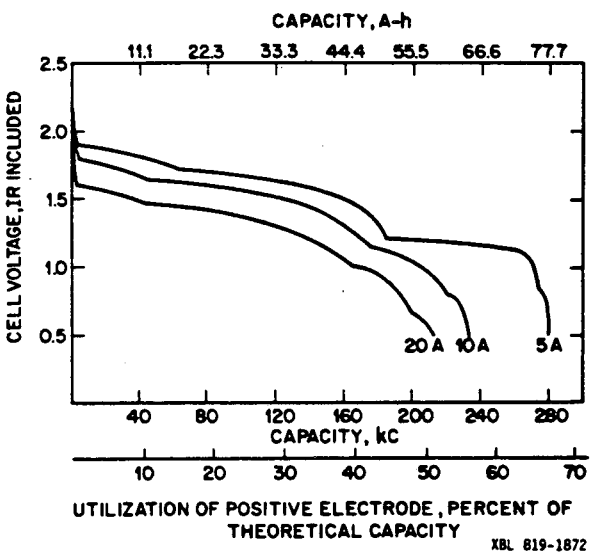

Figure 7. Typical voltage vs. capacity curves for constant current discharges of a $Li_4Si/LiCl$-KCl/FeS_2 cell like that of Figure 6.

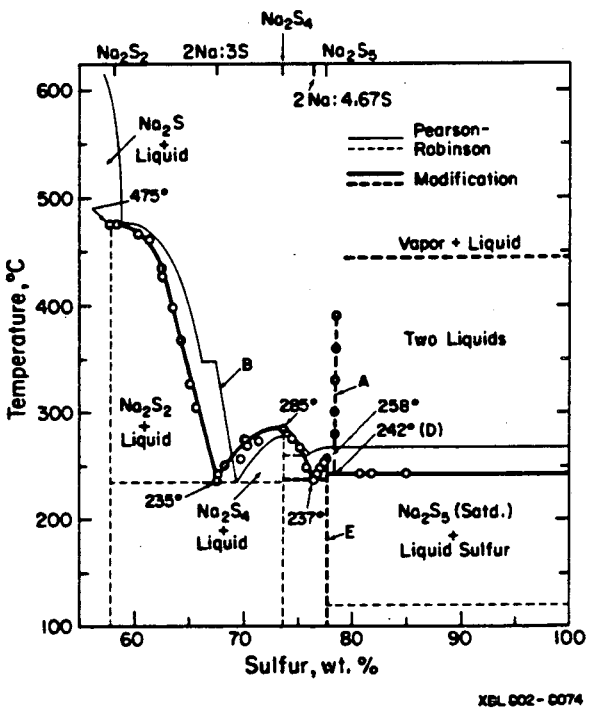

Figure 8. Na_2S_2-S phase diagram according to Oei, Gupta, and Tischer;(27,28) solid circle, data from emf measurements; open circle, data from DTA measurements.

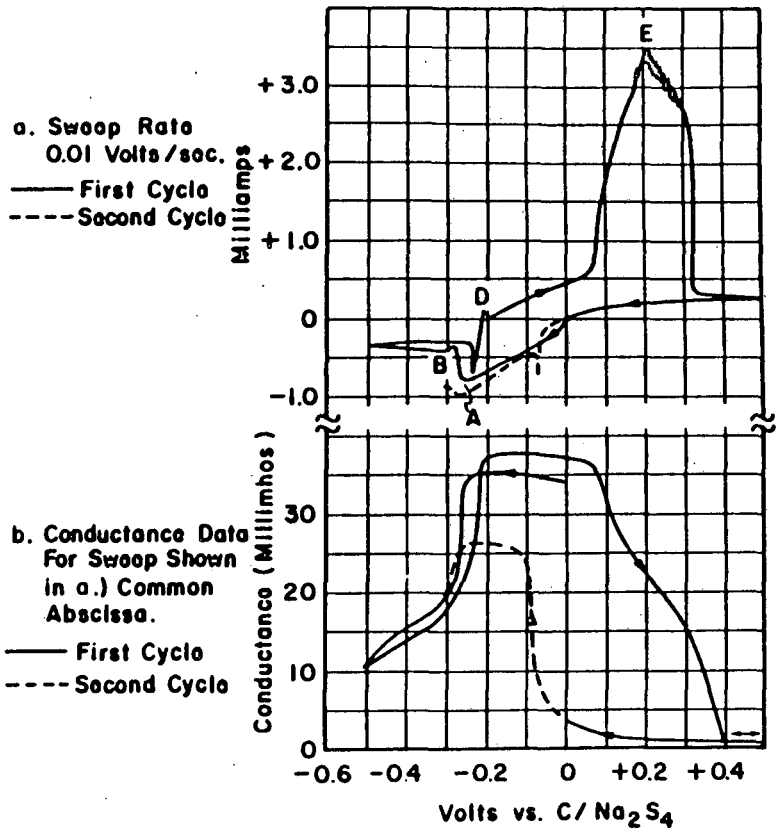

Figure 9. Cyclic sweep and melt conductance in Na_2S_4 at 300°C. Vitreous carbon electrode area is 0.0047 cm^2. Sweep is IR corrected.(37)

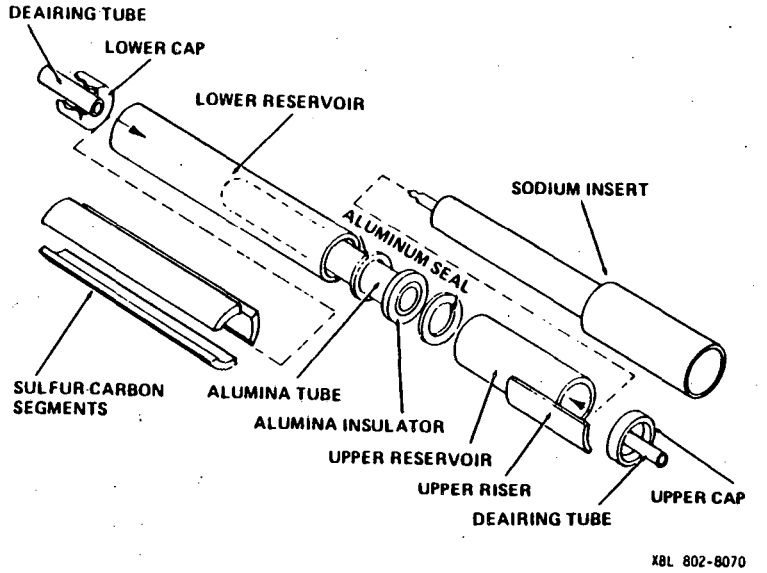

Figure 10. Exploded view of a 168-Ah sodium/sulfur cell of the sodium-core design.

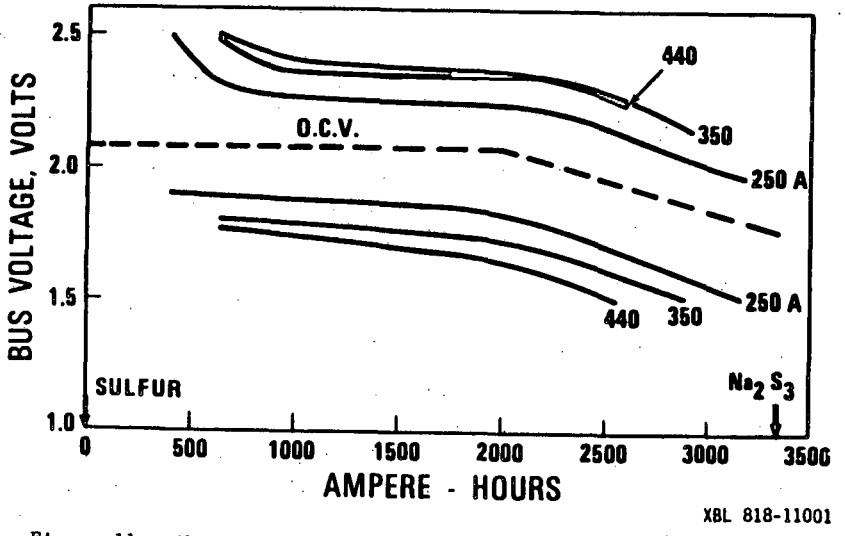

Figure 11. Charge and discharge curves for a 25-cell parallel-connected Na/S battery.

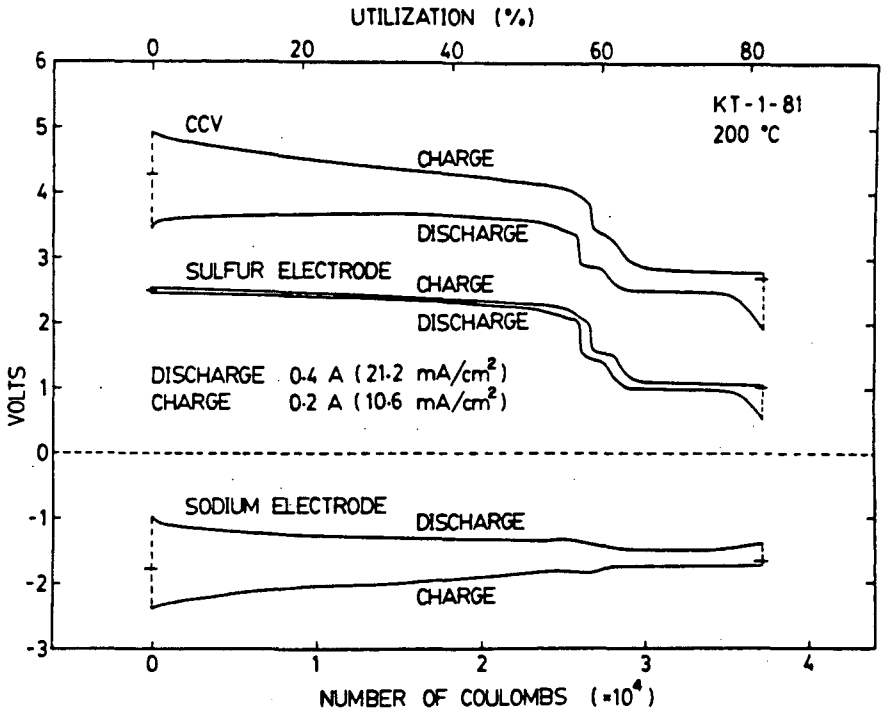

Figure 12. Galvanostatic charge-discharge curve and potentials of sulfur and sodium electrodes vs. Aℓ(III)/Aℓ (in $NaCℓ_{sat.}$ melt) reference electrode at 200°C. Reticulated vitreous carbon used as positive current collector.

TECHNICAL INFORMATION DEPARTMENT
LAWRENCE BERKELEY LABORATORY
UNIVERSITY OF CALIFORNIA
BERKELEY, CALIFORNIA 94720